

Spatial modeling and uncertainty characterization of polymetallic nodules in the Clarion-Clipperton zone

Hari Vishnu, Bharath Kalyan, and Mandar Chitre
Keppel-NUS Corporate Laboratory and Acoustic Research Laboratory,
National University of Singapore
e-mail: {hari, bharath, mandar}@arl.nus.edu.sg

Abstract—Modeling the spatial variation of resources is necessary because it gives an estimate of what to expect during their exploration and exploitation. We focus on the spatial modeling of polymetallic nodules found in the deep sea regions of the Clarion-Clipperton zone in the Pacific. The data from this region available in the open domain is sparse, which warrants modeling techniques that can efficiently use the data to yield reasonable estimates. Additionally, it is necessary to quantify the confidence level of the model’s predictions to aid a user in interpreting them. The confidence level can be captured in the form of an uncertainty map that accompanies the prediction map. We present an approach for modeling of copper percentage variation in nodules found across the Clarion-Clipperton zone. We also describe how the prediction uncertainty given the input features can be estimated.

Keywords—polymetallic nodules, Clarion Clipperton zone, artificial neural network, uncertainty

I. INTRODUCTION

Oceans are natural hunting grounds for resources as land-based sources near depletion. Nowhere is this more evident than the resurging interest in polymetallic nodules (PMN) [1]. PMN are metal concretions formed at several kilometers of depth on the ocean floor. They consist primarily of manganese, iron, nickel, copper (Cu) and cobalt, and also other valuable metal components [2]. Exploration of the Clarion-Clipperton zone (CCZ) in the northeast Pacific region has revealed a significant untapped metal resource potential in the form of PMN deposits [2], [3].

The CCZ is a large area spanning several million square kilometers [4]. However, the PMN deposits in CCZ are not well mapped or quantified yet. In order to plan exploration and exploitation efficiently in such a large area, we need a guiding model of the spatial variation of these resources. This model should be able to estimate variations of nodule resource parameters by utilizing our understanding of the nodule formation process and the limited available distribution data from explorations.

Spatial modeling has been undertaken by several authors previously [5], [6]. In 2003, the International Seabed Authority (ISA) convened a workshop to discuss the modeling of PMN deposits in CCZ, and the discussed bio-geo-chemical mechanisms and models were summarized in an ISA report [4]. It is hard to make exact quantifications of nodule parameters based on these mechanisms because of the vast complexity and interconnectedness of processes leading to nodule formation. What we require is a model that can bridge the observed

variations in the acquired data to the known mechanisms via a data-driven approach. From this perspective, artificial neural networks (ANNs) are ideal tools for modeling of PMNs as they are effective in characterizing unknown underlying variations encountered in data [7]. However, only a few have attempted to tap the power of ANNs for modeling PMNs [4], [8]. In [9], we focused on how to bridge the gap between the known theory and available data on nodules via smart ANN based modeling techniques, with discussion on details that allow a reader to replicate the modeling process. The model predictions were benchmarked against those obtained by ISA [4] and shown to be comparable in accuracy.

While ANNs are capable of yielding predictions by learning patterns in the data, characterizing the confidence level of their predictions is a crucial requirement from a modeler’s point-of-view. This information can guide a model-user on how to interpret the model predictions and what aspects of a model to trust. For example, if an ANN is used to predict nodule parameters in a region where

- 1) data was never gathered before, and
- 2) the environmental factors are significantly different from what the ANN has been trained with,

then the model-user should be flagged that this is uncharted territory for the model.

Another application of uncertainty is as a guide for future data-gathering missions. In our work on PMN exploration, we have been investigating optimal path-planning of exploratory missions to maximize the amount of information obtained from it [10]. An explorer would want to plan missions to explore areas where we are uncertain of the ground realities. This allows us to collect crucial data necessary to improve the model reliability. To do this, we need an uncertainty map of our spatial model predictions.

We present a methodology of ANN-based spatial modeling of the Cu percentage (Cu %) in nodules using the limited data available in the open domain. Furthermore, we describe the estimation of the model’s uncertainty using the dropouts approach. The paper is organized as follows. In section 2, we briefly discuss the formation of nodules, the factors that contribute to this which are used as features in our modeling, and the nodule parameters modeled. In section 3, we discuss the ANN approach to modeling. In section 4, we discuss the characterization of the uncertainty of the predictions. In section 5, we present results of the modeling and uncertainty estimation, and in section 6 we conclude the paper.

II. PMN FORMATION AND FEATURES USED IN MODELING

PMN are formed by accretion of metals in deep-sea regions. The sources for these metals in the waters of the CCZ are primarily terrigenous such as river run-off from the west coast of America (WCA), and volcanogenic metal content injected from sources such as those found along the east Pacific rise (EPR) [4]. The metal particles are ingested by plankton in the photic zone and sink to the bottom as fecal pellets. At the ocean bottom, nodules are formed around a nucleus by entry of these metals through a combination of diagenetic and hydrogenetic processes [11]. Nodule formation at a location is also affected by its depth in relation to the carbon compensation depth, local topography and sedimentation rate [12]–[14]. Local topography and sedimentation rate are key parameters determining small-scale variations in nodule parameters [4], [15].

Based on this understanding, the features selected by us for modeling of nodules are:

1) *Distances from EPR and WCA*: These indicate the distances of the location being considered from the hypothesized terrigenous and the volcanogenic sources of the metals. The metals from these sources may undergo some dilution due to spreading as we move away from the sources [4]. We model this spreading as impacting the nodule parameters in a monotonic way. In order to do this, we follow the approach in our previous work [9] and force our ANN to learn a dependence of the form $c_i \cdot t_i^{p_i}$, where c_i is a constant, p_i is an exponent and t_i is the minimum distance from the source considered. The subscript i can take value of 1 indicating distance from the WCA, and a value of 2 indicating the distance from the EPR. In contrast to [9], we split the effect of WCA and EPR as they contribute different metals which may impact nodule formation differently.

2) *Net primary productivity*: Net primary productivity (NPP) is defined as the flux rate of carbon in plankton due to biological processes [16]. It is an indicator of the photosynthesis activity at the sea surface that contributes metals for nodule formation. The NPP features used in our model were extracted from data computed using a carbon based productivity model [16].

3) *Bathymetry and topography*: Previous attempts to model the effects of topography followed the approach of classifying topographic features into categories like abyssal seamounts, ridges and plains. However, this approach relies on classifications hand-picked by the modeler, and does not quantify the variation in topography. Thus, the performance is heavily reliant on the effectiveness of the manual classification. Instead of this approach, in our modeling we quantify the topographic variation in terms of a set of numerical quantities [9]. These include the depth and the directional depth gradients at each point. The gradient information can help us distinguish the local topography at a location, and modeling dependencies learnt based on these quantities can be interpreted in terms of topographic variations.

The gradients are computed in the following way. Assume that the bathymetric map is available as a function of latitude and longitude as $d(a, b)$, where a denotes the latitude and b denotes the longitude. Also, denote the horizontal distance between two points at lat-long coordinates (a_1, b_1) and (a_2, b_2)

as $H(a_1, b_1, a_2, b_2)$. For any point with lat-long (a, b) , we compute

- First-order depth gradient in eastward direction

$$\Delta_x^1(a, b, \epsilon) = \frac{d(a, b + \epsilon) - d(a, b - \epsilon)}{H(a, b + \epsilon, a, b - \epsilon)}, \quad (1)$$

- Second-order depth gradient in eastward direction

$$\Delta_x^2(a, b, \epsilon) = \frac{\Delta_x^1(a, b + \frac{\epsilon}{2}, \frac{\epsilon}{2}) - \Delta_x^1(a, b - \frac{\epsilon}{2}, \frac{\epsilon}{2})}{H(a, b + \epsilon, a, b - \epsilon)}, \quad (2)$$

- First-order depth gradient in northward direction

$$\Delta_y^1(a, b, \epsilon) = \frac{d(a + \epsilon, b) - d(a - \epsilon, b)}{H(a + \epsilon, b, a - \epsilon, b)}, \quad (3)$$

- Second-order depth gradient in northward direction

$$\Delta_y^2(a, b, \epsilon) = \frac{\Delta_y^1(a + \frac{\epsilon}{2}, b, \frac{\epsilon}{2}) - \Delta_y^1(a - \frac{\epsilon}{2}, b, \frac{\epsilon}{2})}{H(a + \epsilon, b, a - \epsilon, b)}, \quad (4)$$

where ϵ is the lat-long resolution around the point (a, b) chosen for gradient computation. The depth gradients are computed based on bathymetric data obtained from the CCZ region.

4) *Sediment type*: A limited amount of low-resolution data on sediment-type in CCZ is available on some online repositories. The information from these sources is combined and interpolated for use in regions where this data is unavailable. Using the data available, we characterize the sediment-type in terms of fractions of terrigenous material with little biological content, pelagic clay, siliceous sediment and calcareous sediment. For each location, the fractions from these four categories of content are denoted by S_t , S_p , S_s and S_c respectively. We assume that the sediment at any place can be fully characterized by these four types of content. Hence $S_s + S_t + S_p + S_c = 1$.

III. MODELING TECHNIQUE

A. Approach

An ANN is a machine-learning framework based on a network of computational units called neurons which are interconnected by links with multiplying weights [7]. Based on available data, the networks weights can be assigned appropriate values in order to dedicate the network to achieve tasks such as learning, classification and clustering on the data. This process is called training. An ANN is able to take into account several input features which may have complex interconnected effects on the predicted outputs. This makes the ANN ideal for our application. The neurons in an ANN can be organized as layers. These may include an input layer to which the input features are supplied, hidden layers, and an output layer which provides the predicted outputs.

B. ANN architecture and meta-parameters

We use an ANN architecture called a feedforward network which has been extensively employed for pattern recognition tasks in the past. Our ANN contains one input layer, two hidden layers and one output layer. The number of neurons in the first and second hidden layers is 500 and 100 respectively.

TABLE I. SOURCES OF DATA ON FEATURES OBTAINED FROM OPEN-DOMAIN

Feature	Sources
Bathymetry	General bathymetric grid of the ocean [17], [18], Online databases at NCEI [19]
Sediment-type and Cu%	Online databases at NCEI [19], primarily the Seadas database, consisting of: The NOAA and MMS Marine Minerals Bibliography, Archive of Core and Site/Hole Data and Photographs from the Ocean Drilling Program (ODP), NOAA/NOS and USCGS Seabed Descriptions from Hydrographic Surveys, Index to Marine and Lacustrine Geological Samples (IMLGS), Archive of Core and Site/Hole Data and Photographs from the Integrated Ocean Drilling Program (IODP), Archive of Core and Site/Hole Data and Photographs from the Deep Sea Drilling Project (DSDP) and ISA Central Data Repository [20]
NPP (mg C/m ² /day)	Oregon State University [21]

During training of the weights, we minimize the mean square error between the predicted output of the ANN and the expected output, as the cost function. As the nonlinear activation function, we use the rectified linear unit which is shown in the literature to improve ANN generalization performance. The ANN weights are ℓ_2 regularized. We use a learning rate that varies exponentially from 5×10^{-4} to 1×10^{-6} over the progression of the training epochs.

In order to improve the generalization performance of our model using the few data points we have, we expand our dataset by adding synthetic data that represents our prior knowledge of the nodule-forming mechanisms. We generate synthetic data based on the assumption that the relation between the nodule parameters and topography is independent of the direction considered (eastwards/northwards). In other words, the variation learnt by the network with respect to the eastward depth gradients $\Delta_x^1(a, b, \epsilon)$ and $\Delta_x^2(a, b, \epsilon)$, should be the same as that learnt for the northward depth gradients $\Delta_y^1(a, b, \epsilon)$ and $\Delta_y^2(a, b, \epsilon)$ respectively. We encourage the network to learn direction-independent variations by generating additional data from the existing training data by swapping the eastward and northward gradients. This doubles the size of the training dataset and allows the network to generalize topographic variations in a direction-independent way.

To obtain an unbiased estimate of the test performance of the modeling algorithms, we randomly divide the available data into training, validation and test datasets in the ratio 70:15:15. The final model is selected as the one that maximizes the validation performance, which is quantified in terms of regression coefficient on the validation data. The test performance is then calculated as the regression coefficient of the output of this selected model. Since the test points are randomly chosen from all data available for the CCZ, the test performance is indicative of the capability of the ANN to model large-scale variation of the nodule parameters over the CCZ.

C. Parameter modeled and data collection

Cu % is defined as percentage of Cu by weight in nodules found at a location. Modeling this parameter helps determine the feasibility of extraction of this metal after nodule harvesting at a site. Cu is one of the metals in nodule deposits considered to be of economic interest [3]. We model the Cu % conditional on the presence of nodules at a location, referred to as conditional Cu %.

We collected data for modeling from online public sources. The data includes bathymetry, sediment-type, NPP and percentage content of Cu. The sources for this data are shown in table I. We obtained 572 data points for Cu %.

IV. UNCERTAINTY

So how can we characterize the uncertainty of our predictions? Assume we are given a set of locations with known measured values of nodule parameters to within measurement precision. The uncertainty arises when the network is predicting parameters at some *new* location with a set of input features that the ANN has not encountered earlier. The uncertainty of the prediction should be higher when the new set of input features describes a configuration which is further away from the features at known training and validation points. This sort of characterization of uncertainty can be done by visualizing the ANN as a stochastic system which follows a distribution over functions. What we require is an estimate of this distribution that describes our trained ANN. The statistics of that distribution would then quantify the uncertainty of our network.

Some earlier work in the literature showed that an ANN trained using the method of dropouts along with weights regularization, is actually a good estimator of the best possible predictive function based on the given data [22]. Recent work on this by Gal and Ghahramani shows that by using dropouts as a Monte Carlo sampler of the underlying distribution describing our ANN, one can estimate the statistics of the predicted outputs [23]. Dropouts have been well-known in the ANN community for some time as a tool for improving generalization performance. Hence, this approach to estimating the uncertainty of the ANN predictions is simple to use. Since the framework and understanding for incorporating dropouts into ANNs already exists, it is only a matter of reworking this to obtain the uncertainty estimates.

Denote the input feature vector to the ANN as \mathbf{x} and the nodule parameter prediction as y . Denote the best possible predictive function of nodule parameter based on the given training data as $f(\mathbf{x})$, and its distribution conditional on the inputs as $q_f(y|\mathbf{x})$. Our ANN parameterized by weights ω that are trained using dropouts, is a good estimator of this function and is denoted as $\hat{f}_\omega(\mathbf{x})$ [23]. Then, the first and second order statistics of the prediction $y = f(\mathbf{x})$ can be estimated as [23]

$$\mathbb{E}_{q_f(y|\mathbf{x})}[y] = \lim_{T \rightarrow \infty} \frac{1}{T} \sum_{t=1}^T \hat{f}_{\omega_t}(\mathbf{x}_t) \quad (5)$$

and

$$\mathbb{E}_{q_f(y|\mathbf{x})}[y^2] = \tau^{-1} + \lim_{T \rightarrow \infty} \frac{1}{T} \sum_{t=1}^T \left(\hat{f}_{\omega_t}(\mathbf{x}_t) \right)^2 \quad (6)$$

where $\mathbb{E}[\cdot]$ denotes the expectation operator, the subscript t denotes Monte Carlo sampling of the weights ω and input \mathbf{x} via dropouts, and T denotes the number of dropout runs. τ is a precision hyper-parameter which can be computed from

TABLE II. MODELING PERFORMANCE FOR CONDITIONAL CU % USING COMBINATIONS OF DIFFERENT FEATURES AND TECHNIQUES. COLUMNS: A = NPP, B = TOPOGRAPHY, C = SEDIMENT-TYPE, D = t_1 , E = t_2 , F = SYNTHETIC DATA, G = REGULARIZATION

A	B	C	D	E	F	G	Regression coefficient
✓	✓						0.369
✓	✓	✓					0.372
✓	✓	✓	✓				0.376
✓	✓	✓	✓	✓			0.391
✓	✓	✓	✓	✓	✓		0.401
✓	✓	✓	✓	✓	✓	✓	0.410

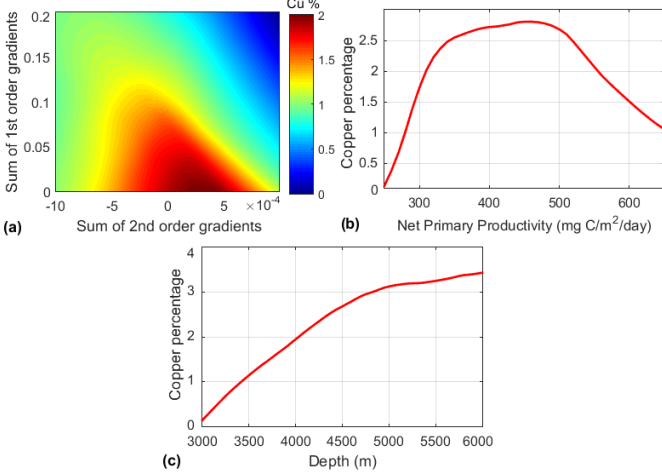


Fig. 1. Modeled variation of conditional Cu % with topographic features. The variation is plotted against (a) $\Delta^1 = \Delta_x^1 + \Delta_y^1$ and $\Delta^2 = \Delta_x^2 + \Delta_y^2$, (b) NPP and (c) depth.

the prior length-scale l , weight regularization parameter λ , dropouts weight retention probability p and number of sample points N as [23]

$$\tau = \frac{pl^2}{2N\lambda}. \quad (7)$$

The variance of the prediction can then be estimated as

$$\text{var}_{q_f(y|\mathbf{x})}[y] = \mathbb{E}_{q_f(y|\mathbf{x})}[y^2] - (\mathbb{E}_{q_f(y|\mathbf{x})}[y])^2. \quad (8)$$

The variance of the prediction y under the distribution $q_f(y|\mathbf{x})$ is in essence a measure of its uncertainty. Thus, the above approach gives us a framework to estimate the uncertainty of our ANN's prediction.

V. RESULTS

We investigate the performance of the regression-based modeling in terms of the average test regression coefficient R , calculated by averaging over four training runs. We investigate the performance improvement obtained by including each of the features mentioned in section II by considering different model configurations using successively larger feature sets, and studying their modeling performances.

The performance of modeling Cu % conditional on nodule presence is summarized in table II. Each row in the table represents a training scenario performed with a certain set of features or modeling techniques such as synthetic data or regularization. The features/techniques used are indicated

by tick-marks in their respective columns. The corresponding test performance is indicated on the right-most column. This interpretation applies to all the tables shown henceforth.

We see that using all the features described in section II improves the modeling performance to some degree. Combining all the input features without using synthetic training data or regularization, yields $R = 0.391$. When we add synthetic data to incorporate directional symmetry, and regularize the weights with an ℓ_2 norm, the performance improves by an additional 4.9% to $R = 0.41$. This is better than the performance of $R = 0.39$ we obtained for the same dataset using the Delaunay triangulation method [24].

In Fig. 1, we briefly study the variations of conditional Cu % learnt by the network with respect to the features we use in the modeling. The model output is averaged over three training runs with high validation performance. Apart from the features against which the variation is plotted, the values of all other features are set to be their averages over the entire collected dataset unless otherwise mentioned. Figure 1 shows that the Cu % is modeled by the ANN as varying non-monotonically with the NPP. The highest predicted Cu % occurs at around NPP = 470 mgC/m²/day. This dependence is similar to the non-monotonic one observed by other models [4]. This variation can be explained by the balance between increasing supply of metals due to increase in NPP, and dilution of metals due to excess biogenous sedimentation. The ANN models that the Cu % increases with depth, suggesting that Cu is found in deeper regions. The variation with topography shows that Cu % is higher in regions with low first-order gradients. These observations indicate that abyssal plains are more favorable to Cu formation. This is consistent with the geological model of entry of Cu into nodules via diagenetic processes, which dominates in regions such as abyssal plains and valleys where sedimentation rates are low.

We generate a prediction map of the conditional Cu % in nodules over the CCZ area using the ANN model trained with all the features. This map is plotted in Fig. 2 (a). In this map and all the maps presented henceforth, the Clarion and Clipperton fractures are represented as two dashed black lines. The trend of the variation predicted by us is somewhat similar to those observed across the entire CCZ described in the ISA report [4]. Some of these predicted features include the band of high Cu % around (11°N, 120°W) and the region (11°N, 125 to 130°W), with a dip around 123°W and 135°W. There is also a region of higher Cu % located at (7.5°N, 154°W) in both maps. Both maps predict that the northern edge of CCZ has much lower Cu %. One difference between the maps is that while our model predicts a band of high Cu % at 140°W spanning from 7°N to 10°N, ISA observes it to be in a smaller region around (8°N, 140°W). Note that ISA does not predict the distribution of Cu % in regions to the east of 119°W.

In Fig. 2 (b), we plot the uncertainty given the inputs, of our prediction map of conditional Cu % over CCZ. The uncertainty is expressed as variance of the estimate. The map in Fig. 2 (b) shows slightly higher uncertainty in some of the western regions. The reason for the uncertainty fluctuations can be partly understood by observing the location of the data points used by us for training, in Fig. 3. We see that some of the regions with high uncertainty such as the northwest region and the patch around (14°N, 119°W) had very few training data

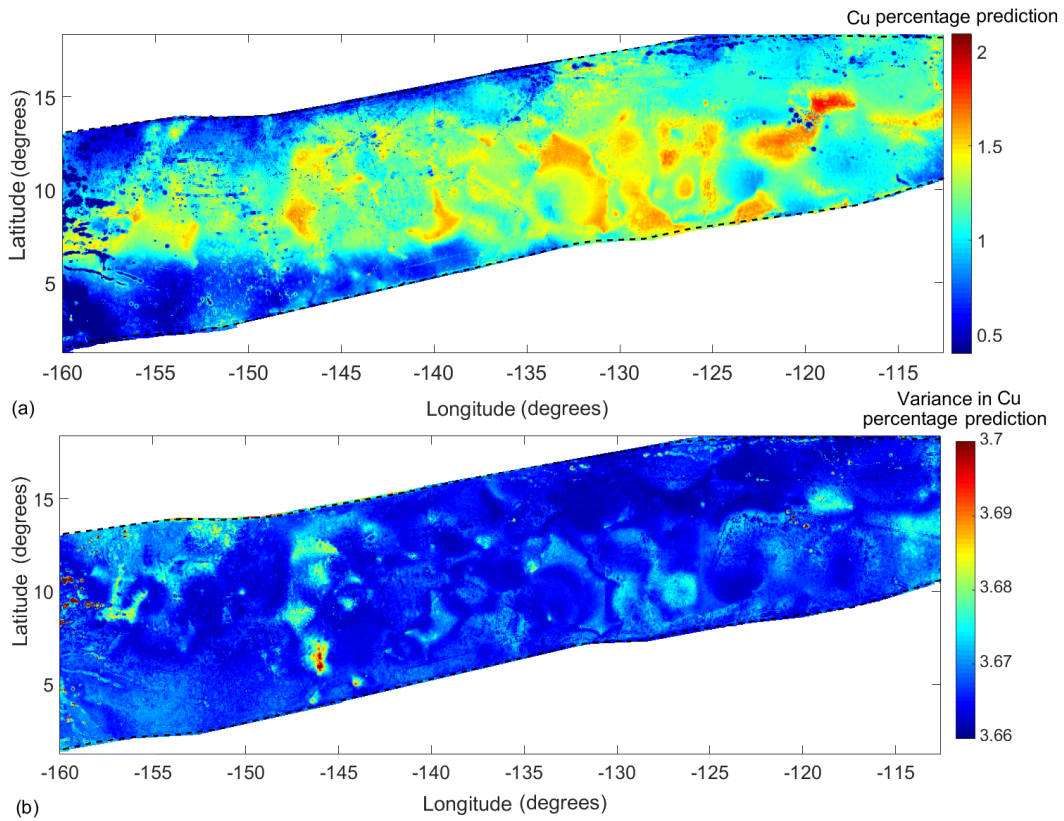


Fig. 2. (a) Predicted variation and (b) variance of prediction of conditional Cu % in CCZ

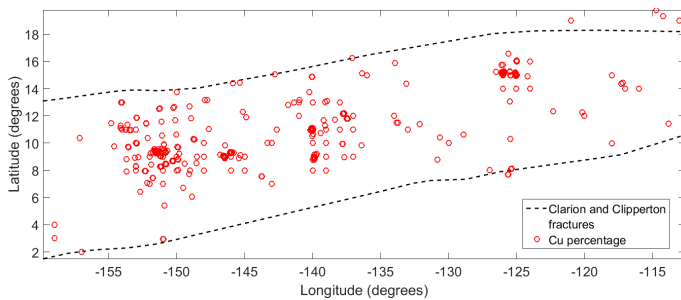


Fig. 3. Distribution of training data samples from CCZ collected from open domain

points. The uncertainty map indicates that the features found in these regions are unfamiliar, so the prediction is achieved through some form of extrapolation. The lower uncertainty at regions like (13°N, 130°W) and (17°N, 115°W) could be because the features in these regions are familiar to the ANN in some way, having been observed at other locations. Thus the ANN is able to make more confident predictions in these regions despite having fewer data points.

In order to better understand the uncertainty variation, we focus on a small portion of the prediction map at a latitude 6.5°N, and spanning from longitudes 149°W to 143°W. Note that there are two training data points at (6.1°N, 149°W) and (7°N, 143°W), but none in between these two. We plot the observed probability densities of the predictions of our Cu %

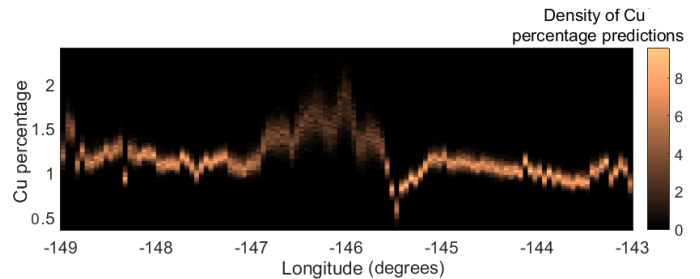


Fig. 4. Probability densities of dropout-based predictions of Cu % from trained model, computed using 5000 dropout runs. Predictions are made along the longitude range 149°W to 143°W, at latitude 6.5°N.

prediction model, computed from 5000 dropout runs. Figure 4 shows the probability densities plotted against the longitude. This plot is representative of the distribution of the ANN's output prediction in this region conditional on the inputs, in between the two training data points. It can be seen that from 147°W to 145.7°W, the densities exhibit fluctuations, larger modes than surrounding longitudes, and are wider. This shows the fluctuations in the prediction output that reflect higher uncertainty. For other points along this longitude range, there are a few data points slightly to the north of 7°N which could be helping lower the uncertainty of predictions.

VI. CONCLUSION

We have outlined how ANN can be used for spatial modeling of Cu % in nodules using the limited data available in the open domain. We believe this work is amongst the first to cover the modeling of this nodule parameter with detailed aspects such as network architecture, meta-parameters used, feature engineering and learning approach. We validated our results by comparing our predictions against those by ISA. The functional patterns learnt by our model match those described by bio-geo-chemical models described in the literature. While the regression performance may not be sufficient to obtain an accurate resource quantification, we believe it can be used for a good initial estimate of the trends we may observe in the CCZ. Hopefully, these can be improved upon with incorporation of more data and use of more efficient modeling techniques such as deep learning methods.

Furthermore, we also described an approach to estimate the model's uncertainty using the dropouts technique. The uncertainty map method flags areas where there is lack of information in terms of features or data points. This uncertainty map is a valuable addendum to the prediction map itself, helping one evaluate the usefulness of the prediction, and utilizing it in further analysis.

VII. ACKNOWLEDGMENT

The authors thank the National Research Foundation, National University of Singapore and Keppel Corporation and for supporting this work done in the Keppel-NUS Corporate Laboratory. The conclusions put forward reflect the views of the authors alone, and not necessarily those of the institutions within the Corporate Laboratory. The authors would also like to thank Mr. Wong Liang Jie for his help in collating some of the data used in this paper.

REFERENCES

- [1] C. Morgan, "Manganese Nodules, Again?" in *Oceans 2011, Kona, Waikoloa*: IEEE, 2011, pp. 1–6.
- [2] G. Glasby, "Deep Seabed Mining: Past Failures and Future Prospects," *Marine Georesources & Geotechnology*, vol. 20, no. 2, pp. 161–176, apr 2002.
- [3] J. Hein, K. Mizell, A. Koschinsky, and T. Conrad, "Deep-ocean mineral deposits as a source of critical metals for high- and green-technology applications: Comparison with land-based resources," *Ore Geology Reviews*, vol. 51, pp. 1–14, jun 2013.
- [4] ISA, "A geological model of polymetallic nodule deposits in the Clarion-Clipperton Fracture Zone," ISA, Tech. Rep., 2010. [Online]. Available: <https://www.isa.org.jm/sites/default/files/files/documents/tstudy6.pdf>
- [5] J. Frazer and M. Fisk, "Geological factors related to characteristics of sea-floor manganese nodule deposits," *Deep Sea Research Part A. Oceanographic Research Papers*, vol. 28, no. 12, pp. 1533–1551, Dec. 1981.
- [6] R. Sharma, N. Khadge, and S. Jai Sankar, "Assessing the distribution and abundance of seabed minerals from seafloor photographic data in the Central Indian Ocean Basin," *International Journal of Remote Sensing*, vol. 34, no. 5, pp. 1691–1706, mar 2013.
- [7] J. Schmidhuber, "Deep Learning in neural networks: An overview," *Neural Networks*, vol. 61, pp. 85–117, 2015.
- [8] A. Knobloch, T. Kuhn, C. Rühlemann, T. Hertwig, K.-O. Zeissler, and S. Noack, "Predictive Mapping of the Nodule Abundance and Mineral Resource Estimation in the Clarion-Clipperton Zone Using Artificial Neural Networks and Classical Geostatistical Methods," in *Deep-Sea Mining*, R. Sharma, Ed. Gewerbestrasse: Springer, 2017, ch. 6, pp. 189–212.
- [9] V. N. Hari, B. Kalyan, M. Chitre, and V. Ganesan, "Spatial modeling of deep-sea ferromanganese nodules with limited data using neural networks," *Journal of Oceanic Engineering (submitted)*, 2017.
- [10] B. Kalyan, V. Ganesan, M. Chitre, and V. Hari, "Optimal point planning for abundance estimation of polymetallic nodules," in *Oceans 2017*. Anchorage: IEEE, 2017.
- [11] P. Halbach, "Processes controlling the heavy metal distribution in Pacific ferromanganese nodules and crusts," *Geologische Rundschau*, vol. 75, no. 1, pp. 235–247, 1986.
- [12] D. S. Cronan, "Controls on the Nature and Distribution of Manganese Nodules in the Western Equatorial Pacific Ocean," in *Marine Minerals: Advances in Research and Resource Assessment*, P. G. Teleki, M. R. Dobson, J. R. Moore, and v. U., Eds. Dordrecht: Springer Netherlands, 1987, pp. 177–188.
- [13] R. A. Kotlinski, "Relationships Between Nodule Genesis And Topography In The Eastern Area Of The C-C region - Meeting of Scientists for the Preparation of a Programme of Work for the Development of a Geological Model of the Clarion-Clipperton Fracture Zone," Nadi, Fiji, Tech. Rep., 2003.
- [14] K. Mewes, J. M. Mogollón, A. Picard, C. Rühlemann, T. Kuhn, K. Nöthen, and S. Kasten, "Impact of depositional and biogeochemical processes on small scale variations in nodule abundance in the Clarion-Clipperton Fracture Zone," *Deep-Sea Research Part I: Oceanographic Research Papers*, vol. 91, pp. 125–141, 2014.
- [15] Y. Ko, S. Lee, J. Kim, K.-H. Kim, and M.-S. Jung, "Relationship between Mn nodule abundance and other geological factors in the northeastern pacific: Application of GIS and probability method," *Ocean Science Journal*, vol. 41, no. 3, pp. 149–161, sep 2006.
- [16] M. Behrenfeld and P. Falkowski, "Photosynthetic rates derived from satellite-based chlorophyll concentration," *Limnology and Oceanography*, vol. 42, pp. 1–20, 1997.
- [17] General Bathymetric Chart of the Oceans website. GEBCO 30 arc-second grid. [Online]. Available: http://www.gebco.net/data_and_products/gridded_bathymetry_data/gebco_30_second_grid/
- [18] P. Weatherall, K. Marks, M. Jakobsson, T. Schmitt, S. Tani, J. Arndt, M. Rovere, D. Chayes, V. Ferrini, and R. Wigley, "A new digital bathymetric model of the world's oceans," *Earth and Space Science*, vol. 2, no. 8, pp. 331–345, aug 2015. [Online]. Available: <http://doi.wiley.com/10.1002/2015EA000107>
- [19] NOAA National Centers for Environmental Information. Main page. [Online]. Available: <http://www.ngdc.noaa.gov/>
- [20] International Seabed Authority. Central data repository. [Online]. Available: <https://www.isa.org.jm/central-data-repository>
- [21] (2015, Nov.) Ocean Productivity. [Online]. Available: <http://www.science.oregonstate.edu/ocean.productivity/index.php>
- [22] N. Srivastava, G. Hinton, A. Krizhevsky, I. Sutskever, and R. Salakhutdinov, "Dropout : A Simple Way to Prevent Neural Networks from Overfitting," *Journal of Machine Learning Research (JMLR)*, vol. 15, pp. 1929–1958, 2014.
- [23] Y. Gal and Z. Ghahramani, "Dropout as a Bayesian Approximation : Representing Model Uncertainty in Deep Learning," *arXiv:1506.02142v1*, vol. 48, pp. 1–10, 2015.
- [24] L. Li and P. Revesz, "Interpolation methods for spatio-temporal geographic data," *Computers, Environment and Urban Systems*, vol. 28, no. 3, pp. 201–227, 2004.